40

SPRAY ATOMIZATION MODELING FOR TABLET FILM COATING PROCESSES

ALBERTO ALISEDA
Department of Mechanical Engineering, University of Washington, Seattle, WA, USA

ALFRED BERCHIELLI
Pharmaceutical Development, Pfizer Global Research & Development, Groton, CT, USA

PANKAJ DOSHI
Chemical Engineering and Process Division, National Chemical Laboratory, Pune, India

JUAN C. LASHERAS
Jacobs School of Engineering, University of California, San Diego, La Jolla, CA, USA

40.1 INTRODUCTION

Film coatings are often used to enhance pharmaceutical tablet products. Tablet film coatings can provide many benefits including improved appearance, added functionality (e.g., sustained release, delayed release, or coatings with active ingredients), brand identity, dose strength identification, ease of swallowing, mask bad taste, improved mechanical strength for improved handling (e.g., during production packaging), and reduce worker exposure (e.g., when dispensing in a pharmacy or hospital setting). There is also potential to improve chemical stability by separation of incompatible ingredients or through reduced oxygen or vapor transmission. Improvements in stability can be significant for maintaining potency, reducing or masking potential color changes in the tablet core, or reducing the development of odor due to chemical reactions. Coating ingredients may also cause instability, so selection of coating components and the coating process conditions are critical for successful product development.

The application of coating material to the tablets is carried out in a complex process that includes four key steps (spray atomization, droplet transport, droplet impact/spreading/drying, and tablet mixing). A schematic of the four elementary processes is shown in Figure 40.1. A photograph of the exterior and close-up view of the corresponding interior of an actual chamber where tablet coating is being performed can be seen in Figure 40.2. First, the coating formulation is atomized into small droplets. This is done by using two-fluid coaxial atomizers in which the liquid formulation is injected through the inner nozzle at low speed and a process gas, typically air, is injected through the outer nozzle at very high speed. The atomizing gas exerts shear and pressure forces on the liquid jet and breaks it into droplets. This type of atomizer allows independent control of the liquid mass flow rate and droplet size. This is because, for all practical liquid flow rates of interest, the liquid speed at the nozzle is low and the breakup process that determines the droplet size is a function of the velocity differential between the two fluids that can be modified by changing the gas speed (i.e., flow rate). The description and modeling of the physics behind this complex process is the focus of this chapter.

The second step in the process is the transport of the liquid droplets onto the tablets' surface. The droplets move under the velocity transferred to them by the atomizing gas and are dried by a secondary flow of hot dry gas that is introduced

Chemical Engineering in the Pharmaceutical Industry: R&D to Manufacturing Edited by David J. am Ende

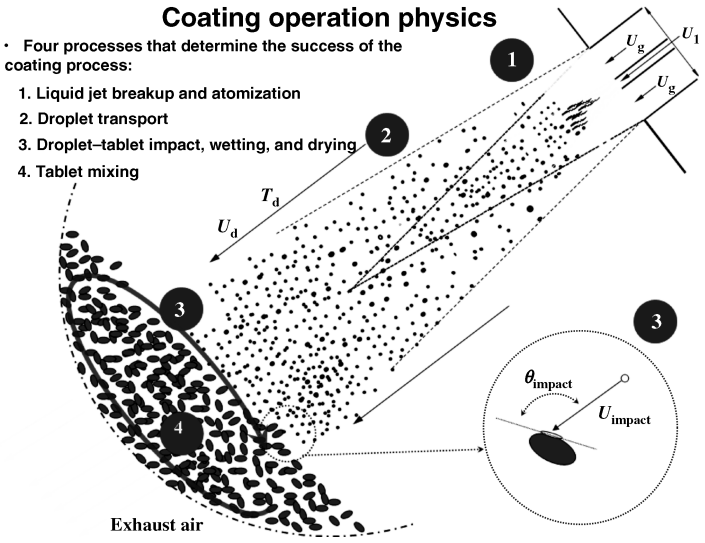

FIGURE 40.1 Schematic of the four elementary processes in the tablet coating operation.

with negligible momentum into the process chamber, so as not to disturb the droplet motion. This secondary gas flow plays the role of providing the energy source needed to balance the latent heat of evaporation of the solvent used in the coating formulation while keeping a sensitive balance between too little drying (droplets hitting the tablets with too much solvent) and too much drying (droplets drying out entirely during their transport). The third step is the impact and spreading of the droplets onto the tablets. The droplet spray hits the tablets at or near the surface of the bed. By rotating through the bed in a random manner, the individual tablets form a continuous film coating by integrating the effects of many tiny droplets that hit them at different times during the process. This last aspect forms the fourth elementary process that determines the success of the operation. For the droplet spreading on the individual tablets to lead to a uniform film coating, the tablets need to be adequately mixed in their recirculating porous bed.

While there are extensive studies in the pharmaceutical literature on the granular flow mechanics that dominate mixing in the tablet bed, evaluation of coating quality and properties, and the thermodynamics that set droplet and tablet drying [1–8], much less attention has been paid to the atomization process [9–12]. Mathematical modeling of all four aspects of tablet film coating is important and has far-reaching impact on the economics of pharmaceutical commercialization, potentially reducing both cost and time to market. Generally, this is the last unit process where a batch

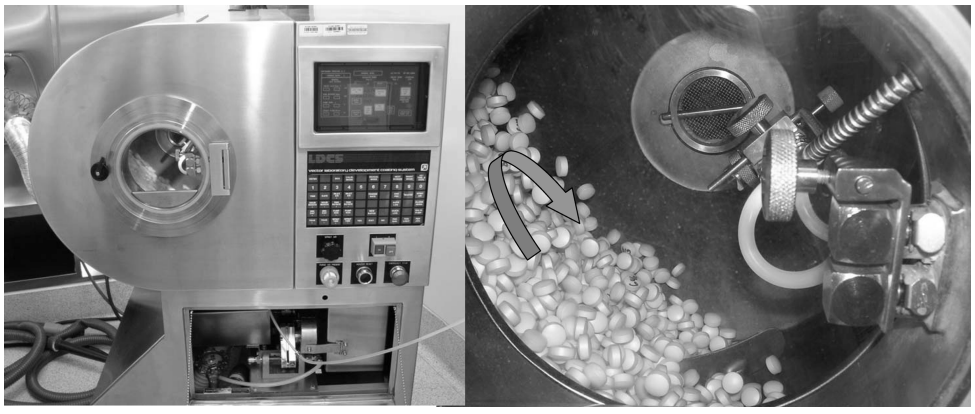

FIGURE 40.2 *Left*: External view of Vector Corporation Laboratory Development Coating System (LDCS 20/30). *Right*: Internal close-up view of cascading tablets during a development coating run. *Note*: In the image above on right, a clear coating is added to white tablets. Numbers have been added to track individual tablets during the development coating run. The arrow indicates the direction of tablet movement.

may be rejected if process conditions are poorly selected or controlled resulting in an unacceptable defect rate. Tablets with surface defects may be removed from the batch after a complete visual quality inspection; however, this added step is time-consuming and should be avoided.

Tablet coating has evolved throughout history from sugar-based coatings, to solvent-based polymeric film coatings, to today's aqueous-based polymeric film coatings. Equipment preferences have also changed from nonperforated pans to partially perforated and fully perforated pans. Coating application has also drastically improved from ladling of sugar coatings to films applied with modern pneumatic or coaxial air blast spray guns. This chapter describes advances in mathematical modeling of the atomization process that enable droplet size predictions, based on models of the physical processes that control liquid jet breakup in two-fluid coaxial atomizers, for pharmaceutically relevant aqueous and organic polymeric film coatings.

In the process control and experimentation that is involved in the design and scale-up of coating operations, atomization is one of the most difficult elements to understand and optimize. Direct measurements of droplet size are typically not available during coating operations and scale-up studies. In addition, droplet size effects are often masked during development trials by the large variability in the results associated with the wide ranges of liquid and gas flow rates and velocities that need to be investigated. Predicting the size of the coating formulation droplets resulting from the atomization process is essential to the success of the coating process, as small droplets can dry and lead to reduced coating efficiency, or they may fail to coalesce on the tablet surface, not producing a smooth continuous film. Droplets that are too large, on the other hand, can see reduced solvent evaporation and lead to overwetting. This causes coating defects (e.g., sticking marks where tablets contact each other and stick together or rough coatings due to erosion of the tablet core components). Similarities between the effects of droplets below or above the valid size range make the diagnosis of these defects difficult.

As we will show in the following sections, droplet size is a function of fluid properties (e.g., surface tension, viscosity), atomizer geometry (e.g., liquid and gas nozzle diameters), and process conditions (e.g., liquid and gas flow rates). The selection of a coating formulation for a specific pharmaceutical tablet is influenced by many factors that may be unrelated to the physical processes involved. Once approved by regulatory agencies, however, changes to the formulation are not made unless necessary and often require justification and supporting regulatory data. The scale-up process, or changes in the industrial tablet manufacturing process that may occur during the lifetime of the product, may require modifications in atomizer geometry or process conditions. Under these circumstances, the atomization of the coating formulation will change. Unless a physics-based model is available to predict the direction and magnitude of those changes, a costly and time-consuming process is required to adapt the coating conditions to the new setup. These full-scale trials represent a major disruption to the manufacturing and commercialization, particularly if active ingredient costs are high, or the delays lead to reductions in product supply.

The atomization process is a key part of the tablet coating process used in the pharmaceutical industry. It is therefore of great importance to develop physics-based atomization models that can predict droplet size and volume density as a function of fluid properties, atomizer configuration, and process conditions. These models can play an important role in the design of the process, including selection of equipment and process parameters, and in the optimization at all different levels: lab, pilot, and full scale. In the following sections, we will discuss the rheology of coating formulations, characterization of coating suspensions and solutions, detailed physics of atomization and the associated equipment, droplet size and velocity measurement, a mathematical model for mean droplet size, insight into the scale-up of the coating operation, and some conclusions on the current state and future directions of this technology.

40.2 COATING FORMULATIONS, PHYSICAL PROPERTIES, AND RHEOLOGY CHARACTERIZATION

Coating formulations typically contain significant amounts of polymers, plasticizers, surfactants, pigments/colorants, antifoaming, antitack ingredients, film modifiers (i.e., sugars), and opacifiers. Because of this high content of large molecules in solution or of solids in colloidal dispersion (e.g., titanium dioxide, talc), coating fluids have complex rheology, exhibiting non-Newtonian behavior during the atomization process.

Tablet film coatings can be soluble (e.g., color coatings for immediate release formulations), insoluble (e.g., enteric coatings that are insoluble at gastric pH), or partially insoluble (e.g., porous or semipermeable membranes that may contain insoluble and soluble ingredients). Immediate release coating formulations are commonly based on polymers such as hypromellose (also known as hydroxypropyl methylcellulose or HPMC) and polyvinyl alcohol (PVA), but other polymers or natural products such as shellac have also been used. Functional coatings for controlled release are often based on polymers such as cellulose acetate, ethyl cellulose, or methacrylates. In this chapter, we will present experimental results obtained from two characteristic coating formulations for immediate release tablets: HPMC (Colorcon Codes: Y-30-18037, OY-LS-28914) and PVA (Colorcon Code: 85F18422), and a characteristic coating for controlled release that is composed of a mixture of cellulose acetate/polyethylene glycol and forms a semipermeable

TABLE 40.1 Example Coatings Discussed in This Chapter

Coating Number	Abbreviation	Vendor Code or Components	Composition
1	Opadry II White-HPMC	Colorcon Code: Y-30-18037	15% solids, 85% water
2	Opadry II White-PVA	Colorcon Code: 85F18422	20% solids, 80% water
3	Opadry II White-HPMC	Colorcon Code: OY-LS-28914	10%, 12%, 15% solids; 90%, 88%, 85% water
4	CA-PEG	Cellulose acetate 398-10	8%
		Polyethylene glycol 3350	2%
		Acetone	87%
		Water	3%

membrane allowing osmotic drug delivery [13, 14]. Table 40.1 lists these examples of coating formulations discussed in this chapter.

As we have pointed out in the previous sections and will show in the formulation of a mathematical model for the breakup of the liquid into individual droplets, the atomization process that constitutes the first stage of the pharmaceutical coating operation is strongly influenced by the physical properties of coating solutions. The two key nondimensional parameters that control this process are the Weber number ($We = \rho_g U_g^2 d/\sigma$) and the Ohnesorge number ($Oh = \mu_l/\sqrt{\rho_l \sigma d}$), where ρ_g is the gas density, U_g is the gas velocity at the nozzle, d is the liquid jet diameter, μ_l is the liquid viscosity, ρ_l is the liquid density, and σ is the value of the surface tension between the liquid and the gas. The Weber number represents the relative importance of the inertia of the high-speed gas stream that disturbs the liquid jet and the surface tension stresses that minimize surface energy, bringing cohesion to the liquid. The Ohnesorge number characterizes the relative importance of viscous and surface tension stresses. Clearly, the characterization of the physical properties of the coating fluids is a key preliminary step in the understanding and modeling of the liquid atomization in the tablet coating processes.

40.2.1 Coating Solution Viscosity Measurement

A typical film coating formulation usually contains a mixture of solids comprising of polymer, plasticizer, pigment/opacifier, and other film modifiers dissolved in water or a nonaqueous organic solvent. The coating formulations could either be a solution if solids are soluble in the solvent or else they could form a colloidal suspension. Figure 40.3 shows the viscosity for four previously mentioned coating fluids at 25°C for different shear rates. These fluids show slight shear thinning behavior (i.e., viscosity decreases with increasing shear rate), up until shear rate reaches $200\,s^{-1}$. However, beyond this value of shear rate, viscosities are almost constant. In a typical atomization process, the shear rate is well above $200\,s^{-1}$ [9], so coating solution viscosity can be assumed to be constant for a given coating formulation.

40.2.2 Effect of Solids Content on Viscosity

Figure 40.4 shows the variation of viscosity for coating 3 with increasing solids content. For this formulation, the viscosity at low solids content, that is, up to 5%, is quite close to that of the solvent. However, with further increase in solids content, the viscosity increases in an exponential fashion, typical of this type of colloidal dispersion.

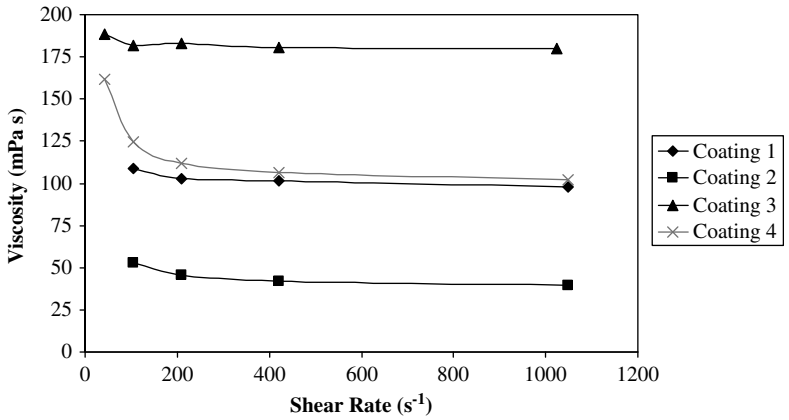

FIGURE 40.3 Viscosity versus shear rate for four coating formulations at 25°C.

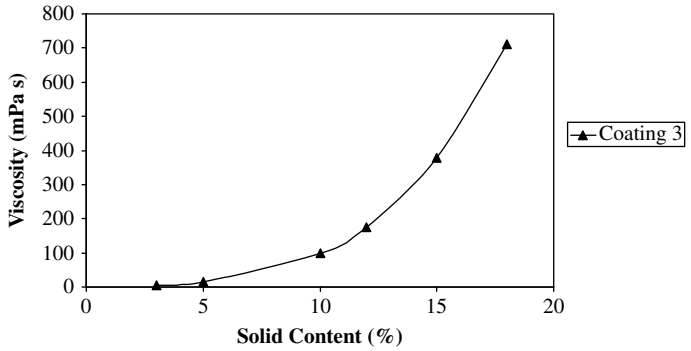

FIGURE 40.4 Solution viscosity versus solids content for coating 3 at 25°C and a shear rate of $1000\,s^{-1}$.

40.2.3 Effect of Temperature on Coating Solution Viscosity

Figure 40.5 shows the variation of viscosity of three different coating fluids with temperature. The viscosity of all three fluids decreases linearly with increasing temperature. The viscosity reduces to almost half their values when the fluids are heated from 20 to 35°C. This behavior can be taken advantage of, by heating very viscous coating formulation prior to injection in the atomizer, to facilitate tablet coatings with very high solids content, where the high viscosity makes atomization difficult. At the same time, this points out the need to monitor thermal gelation point of coating formulations, since operating conditions that include temperatures above that threshold will lead to semisolid and almost unsprayable coating fluids [15].

40.2.4 Coating Solution Surface Tension Measurement

Table 40.2 shows the surface tension data for different coating fluids and their respective solvents measured at approximately 23°C. The values of surface tension for all the aqueous coating fluids (1–3) are quite close to each other, irrespective of the solids concentration. However, they are quite low compared to the surface tension of the solvent (water). This observation is not true, however, for the coating formulation with organic solvent (acetone). These data are in accord with the finding in the literature that HPMC acts as a surfactant and reduces the surface tension of water for very low concentrations ($\sim 2 \times 10^{-5}$% w/w) [15]. After this point, further increase in HPMC concentration has little effect on reducing the surface tension. This behavior is similar to the critical micelle concentration shown by surface-active materials. The typical composition of coating formulations leads to surface concentrations that are always above this threshold, so the saturation effects in the values of surface tension found in our experiments are characteristic of these types of coatings.

40.3 SPRAYING PROCESS AND EQUIPMENT

As highlighted in previous sections, the atomization of coating liquid formulations into small droplets is a key step in the process of pharmaceutical tablet coating and the focus of this chapter. To contribute to success in the coating operation, atomization of the coating formulation must

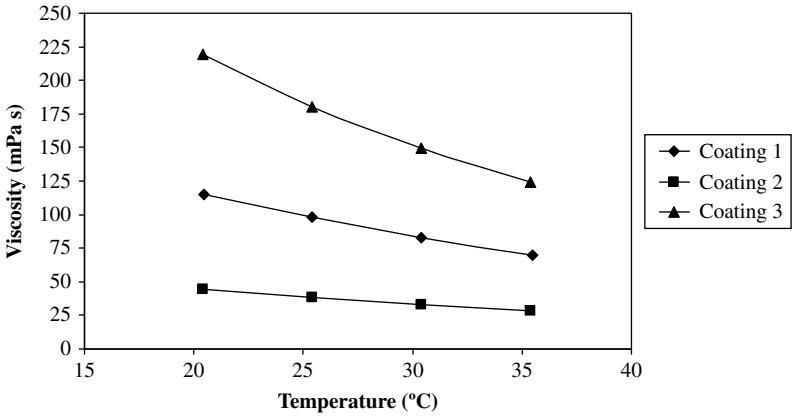

FIGURE 40.5 Effect of temperature on viscosity of coating solutions.

TABLE 40.2 Effect of Solids Concentration on the Viscosity, Density, and Surface Tension of Coating Fluids Measured

Coating No.	Coating Type	% Solids	Viscosity of Coating Fluid @25°C and 1048 s^{-1} (kg/m s)	Density of Coating Fluid (g/cc)	Density of Solvent (g/cc)	Surface Tension of Coating Fluid (dyn/cm)	Surface Tension of Solvent (dyn/cm)
1	Opadry II White (Y-30-18037), HPMC/lactose/ TiO_2/triacetin/water	15	0.098	1.05	1.00	46.98	72.8
2	Opadry II White (85F18422), PVA/PEG/water	20	0.039	1.07	1.00	43.93	72.8
3	Opadry II White (OY-LS-28914), HPMC/lactose/ TiO_2/triacetin	10	0.095	1.02	1.00	48.22	72.8
3	Opadry II White (OY-LS-28914), HPMC/lactose/ TiO_2/triacetin	12	0.181	1.03	1.00	47.66	72.8
3	Opadry II White (OY-LS-28914), HPMC/lactose/ TiO_2/triacetin	15	0.419	1.04	1.00	46.67	72.8
4	CA/PEG/acetone/ water	10	0.102	0.82	0.79/1.00	29.71	29.7

provide controllable droplet size distributions for a wide range of liquid flow rates. In addition, the concentration of droplets across the spray should be spatially uniform. These two requirements make two-fluid coaxial atomizers the most common in this setting. Unlike pressure atomizers, commonly used in diesel fuel injection, where the size of the liquid droplets depends on liquid flow rate, two-fluid atomizers allow control of the droplet size independent of liquid flow rates. In its simple configuration, they produce a very predictable spatial distribution of droplets within the spray, with a significant radial gradient of concentration, and high uniformity along concentric rings. To improve the spatial uniformity of the droplet flux, two auxiliary gas jets are used. In the atomizer design, these side jets are located at a small distance from the nozzle, diametrically opposed to each other, breaking the cylindrical symmetry of the coaxial atomizer and creating two symmetry planes. Because they help shape the flow of gas and liquid droplets from the atomizer, these side jets are commonly referred to as pattern air. The spray takes on an elliptical cross section, consistent with the two symmetry planes, and the droplet spatial distribution becomes very homogeneous.

Spray guns typically used in tablet spray coating include Schlick, Spraying Systems, Freund, Binks, and Walther Pilot. Typical spray gun designs can be seen in Figure 40.6 (front view of a Schlick fluid nozzle and air cap setup for creating an elliptical spay pattern), Figure 40.7 (side view of a Schlick fluid nozzle and air cap setup), Figure 40.8 (front view of a Spraying Systems fluid nozzle and air cap setup for creating an elliptical spray pattern), Figure 40.9 (side view of a Spraying Systems fluid nozzle and air cap setup), Figure 40.10 (front view of a Spraying Systems fluid nozzle

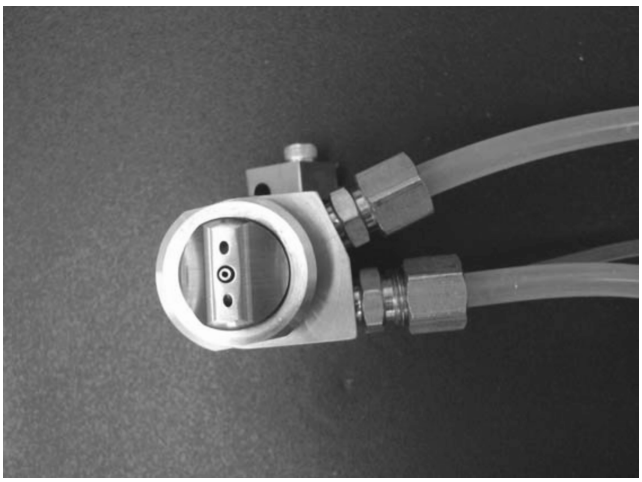

FIGURE 40.6 Front view of a laboratory-scale spray gun for tablet coating (Schlick fluid nozzle and air cap with spray gun body by Vector Inc.).

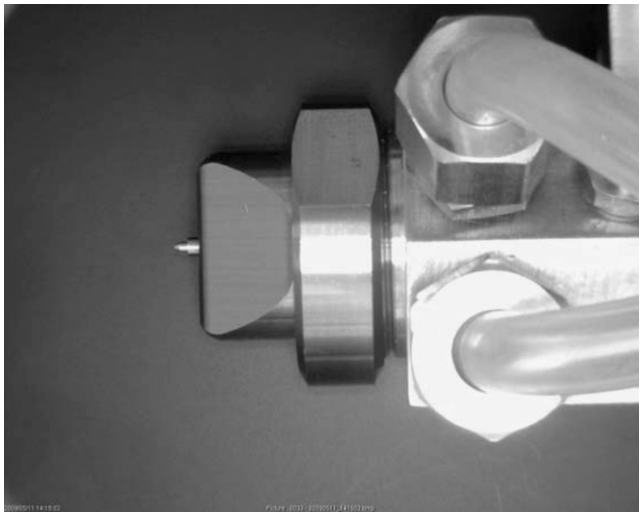

FIGURE 40.7 Side view of a laboratory-scale spray gun for tablet coating (Schlick fluid nozzle and air cap with spray gun body by Vector Inc.).

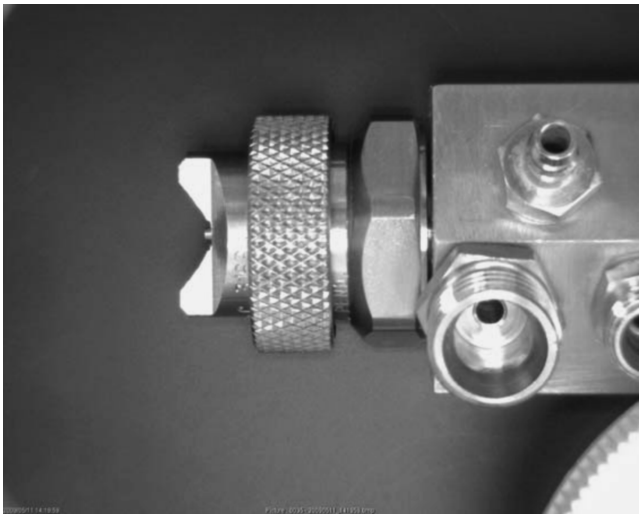

FIGURE 40.9 Side view of a laboratory-scale spray gun for tablet coating (Spraying Systems fluid nozzle and air cap with spray gun body by Vector Inc.).

and air cap setup for creating a round spray pattern), Figure 40.11 (side view of a Spraying Systems fluid nozzle and air cap setup). Figure 40.12 provides a sketch of the spray nozzle showing key geometric parameters that must be provided to successfully model the atomization process.

The use of side gas jets in pharmaceutical coating atomizers also improves spray coverage. This is defined as the cross-sectional area of the spray where it intersects with the tablet bed. This area, which is obviously determined by the distance from the spray gun to the tablet surface and the spray shape, is important because it determines the probability of a tablet moving along the surface of the tablet bed to collide with one or more coating formulation droplets. By stretching the spray in the direction perpendicular to the tablet motion (major axis of the spray elliptical cross section) and reducing the coverage in the perpendicular direction (minor axis of the ellipse), pattern air increases the number of tablets that will receive the impact of coating droplets as they are distributed on the tablet bed's surface, since it increases the width covered by the spray. At the same time, the shorter coverage along the trajectory of the tablets reduces the probability of a tablet being hit by too many droplets over a short time while it traverses the spray in its motion, thereby reducing the likelihood of overwetting or tablets sticking to each other.

Coating operations requires atomization to work efficiently over a wide range of operating conditions. Poor selection

FIGURE 40.8 Front view of a laboratory-scale spray gun for tablet coating (Spraying Systems fluid nozzle and air cap with spray gun body by Vector Inc.).

FIGURE 40.10 Front view of a laboratory-scale spray gun for tablet coating (Spraying Systems fluid nozzle and air cap with spray gun body by Vector Inc.).

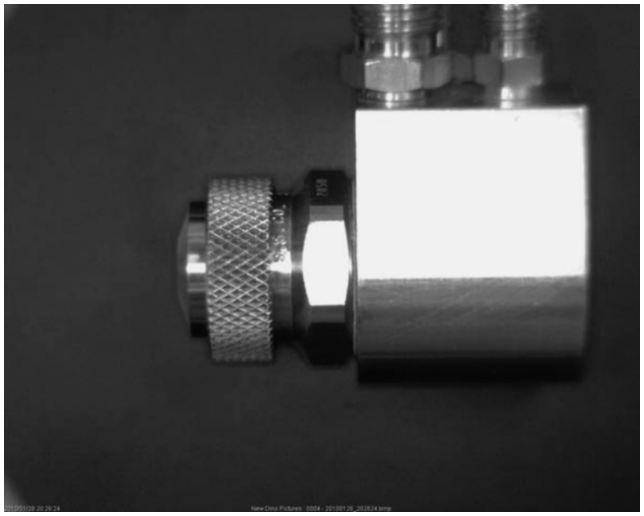

FIGURE 40.11 Side view of a laboratory-scale spray gun for tablet coating (Spraying Systems fluid nozzle and air cap with spray gun body by Vector Inc.).

or poor control of process conditions can lead to nonoptimal results (i.e., poor coating appearance, tablet core erosion, tablet breakage, potency loss, or dosage form functionality changes) or potentially batch failure. Successful tablet coating requires selecting the appropriate tablet formulation components, tablet properties, coating formulation, coating properties, and coating process conditions. The liquid flow rate (i.e., spray rate) needs to be determined in combination with the appropriate thermodynamic [2] drying conditions (air flow, temperature, and humidity), so that evaporation of the solvent occurs at an adequate rate (too much evaporation leads to dry droplets not spreading over tablets, while too little leads to overwetting). Spray rate and coating formulation solid content determine the total flux of coating material onto the tablets, and, therefore, these two parameters need to be selected in conjunction to control the overall coating time. There is a minimum number of passes through the spray that a tablet needs to go through in order to develop a uniform coating. Longer spray times allow for increased passes of tablets under the spray zone and when combined with good mixing and appropriate tablet shape selection results in improved intratablet and intertablet coating uniformity; however, an efficient process should not be longer than is required to ensure product specifications are met. Changes in spray rate or coating fluid solids content will affect the droplet size of the atomized coating. Other atomization parameters need to be adjusted to maintain optimal droplet size under these changing conditions. Predictive models and accurate measurements of process conditions are essential to minimize the challenges presented by the wide range of needs within the coating operation. Manufacturers of atomization equipment typically provide values of the atomization and pattern air pressures as the key process settings because they are easy to measure in the industrial environment. These are, however, surrogates for the gas flow rates that play a key role in the atomization process and droplet redistribution within the spray. Different atomizer setups inside the coating equipment may translate to different pressure losses from the measurement to the atomizer head, introducing uncertainty about the actual flow rates in the process. It is, therefore, preferable to measure volumetric flow rates for both atomizing and pattern air. Air flow rates can economically be measured with rotameters (i.e., a graduated meter consisting

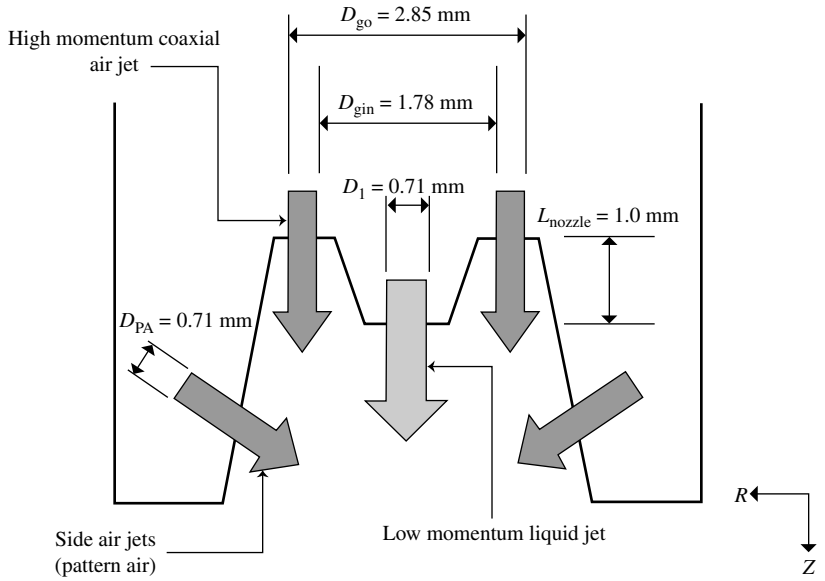

FIGURE 40.12 Side view sketch of a laboratory-scale spray gun for tablet coating (Spraying Systems fluid nozzle and air cap with corresponding measurements used in modeling).

of a tapered tube containing a free float for air flow measurement). The Key Instruments Flo-Rite Series is an example of a commercially available rotameter. Volumetric flow rates of air can also be measured with mass flow meters providing a digital output that is easy for the operator to read and allows coaters with data collection capabilities to store atomization and pattern air flow values electronically. The Sierra Top-Trak 824 series is an example of a mass flow meter. A combination of the appropriate monitoring equipment and accurate physics-based models greatly improves the effectiveness and efficiency of coating operations.

40.4 DROPLET SIZE AND VELOCITY MEASUREMENTS

The result of the atomization process described in previous sections, and modeled mathematically in the next section, is a distribution of droplets with a wide range of diameters and velocities. The combination of these two properties determines the droplet inertia and therefore how the droplets interact with the underlying high-speed turbulent air jet in which they are immersed. These interactions, together with the initial conditions for the motion of the droplets, will ultimately shape the spray coating process, setting the values of the droplet number density, droplet velocity at the impact with the tablet bed, and mass flux per unit area. These fluid variables determine the fate of individual droplets impacting on the tablets and, when ensemble over the whole droplet distribution, the success of the coating operation.

The droplet size distribution is given by the balance between cohesive forces, such as surface tension and viscosity, and disruptive forces, namely, pressure and shear forces exerted on the liquid surface by the atomizing gas stream. Because of the turbulent character of the high-speed gas stream and the nature of the instability with a wide range of unstable wavelengths with similar growth rates, the resulting droplets have a distribution of sizes, not a unique diameter as expected in other types of liquid breakup such as Rayleigh–Plateau instability [16]. Because of this, measurements and modeling of the droplet size are focused on characterizing the full distribution of diameters. One way to do this is to describe the different statistical moments of the distribution of diameters. Table 40.3 gives the mathematical definition and physical interpretation of the most used moments of the size distribution.

Droplet size distributions can be measured by a number of instruments that rely on light scattering to determine the droplet size unintrusively. The most widely used measurement technique is based on light interferometry to evaluate the phase shift introduced by a scattering spherical droplet on the fringe pattern created by the superposition of two laser beams with slightly different frequencies. This phase shift is proportional to the scatterer's diameter. A much more detailed description of the measurement principle was published by Bachalo [17]. This measurement technique has the added advantage that with some further processing of the information in the collected light scattered by the droplets, it also provides the droplet velocity distribution from the Doppler frequency shift. Although the physical principles

TABLE 40.3 Mathematical Definition and Physical Interpretation of the Most Used Moments of the Size Distribution

Statistical Moment	Mathematical Definition	Physical Meaning
D_{10}	$d_{10} = \frac{\sum_{i=1}^{N} n_i \cdot d_i}{\sum_{i=1}^{N} n_i}$	Diameter of the droplet that represents the arithmetic average of all droplet diameters. d_i is the diameter of droplets in size bin i and n_i is the number of droplets in that bin of the distribution
D_{20}	$d_{20} = \sqrt{\frac{\sum_{i=1}^{N} n_i \cdot d_i^2}{\sum_{i=1}^{N} n_i}}$	Characteristic diameter that if all droplets were this same size (monodisperse), they would contain the same surface area as the whole distribution under study
D_{30}	$d_{30} = \sqrt[3]{\frac{\sum_{i=1}^{N} n_i \cdot d_i^3}{\sum_{i=1}^{N} n_i}}$	Characteristic diameter that if all droplets were this same size (monodisperse), they would contain the same volume (or mass) as the whole distribution under study
D_{32}	$d_{32} = \frac{\sum_{i=1}^{N} n_i \cdot d_i^3}{\sum_{i=1}^{N} n_i \cdot d_i^2}$	Characteristic diameter that if all droplets were this same size (monodisperse), they would have the same volume to surface ratio as the whole distribution under study
D_{50}	$\frac{\sum_{i=1}^{M(D_{50})} n_i \cdot d_i^3}{\sum_{i=1}^{N} n_i \cdot d_i^3} = 0.5$	Characteristic diameter for which all droplets smaller than this contain 50% of the volume (or mass) of the whole distribution under study. M is the bin for which the cumulative volume summation reaches 50% of the total. The diameter corresponding to that bin is d_{50}
D_{90}	$\frac{\sum_{i=1}^{L(D_{90})} n_i \cdot d_i^3}{\sum_{i=1}^{N} n_i \cdot d_i^3} = 0.9$	Characteristic diameter for which all droplets smaller than this contain 90% of the volume (or mass) of the whole distribution under study. L is the bin for which the cumulative volume summation reaches 90% of the total. The diameter corresponding to that bin is d_{90}

behind these measurements are well established, the technological details involved in getting robust, accurate measurements in a wide variety of operating conditions are extremely complicated. There are currently only two instrument manufacturers that provide commercial solutions based on this technique: TSI Inc., Shoreline, MN (PDPA (phase Doppler particle analysis)) and Dantec Dynamics A/S, Skovlunde, Denmark (PDA (phase Doppler anemometry)).

The characteristics of the droplets in the spray vary spatially both radially and axially. The latter dependency is easy to describe and is universal for different spray types, with different phenomena having different relative weights in the resulting droplet distribution. An example of this axial evolution is shown in Figure 40.13. In the close proximity of the nozzle, droplets are very large or are growing to a large diameter. In this region, the liquid jet has been shattered by the atomizing air and large liquid masses, not necessarily spherical in shape, are being stripped from the liquid core. As these liquid masses get deformed by the high-speed gas stream, they take on shapes with low curvature that looks to the particle sizing measurements as increasingly large droplets. It is not until the deformation stage ends and the breakup into smaller droplets begins that the shape becomes truly spherical and accurate measurements are possible. This happens in the region between 5 and 10 diameters downstream. After this region, the breakup proceeds with the droplet diameter decreasing sharply before it plateaus in the region between 20 and 30 diameters. At this point, the breakup process has finished. The breakup of the liquid into smaller droplets makes surface tension a stronger cohesive force. Together with the dilution of the high momentum jet by expansion of its cross-sectional area due to entrainment, the balance between disruptive and cohesive forces tilts very soon toward the cohesive side, thereby stopping the breakup. From a practical point of view, this process usually takes place within the first 2 in. of the jet, giving rise to a minimum standoff distance between the coating gun and the tablet bed, since the coating is designed to impact spherical droplets that are small and do not extend beyond the boundaries of a single tablet. In the region beyond where breakup takes place, the droplet size is dependent on secondary processes that determine the dynamics of small spherical droplets immersed in a turbulent gas jet. At this stage, the evolution of the droplet size distribution can be evaluated with a population dynamics equation [18] where the sources on the right-hand side are turbulent transport, coalescence, and evaporation. Typically, these phenomena alter the droplet diameter very slowly in the range of interest for the coating operation, as seen by the constant mean diameter measured in the second half of the plot in Figure 40.13 (between 25 and 50 diameters downstream).

The evolution of the radial distribution of droplet sizes is determined by the different response of droplets to the high-speed gas flow due to their different inertia. The larger droplets are found along the centerline, where they maintain their strong axial momentum communicated by the high-speed jet near the nozzle. Smaller droplets have lower inertia

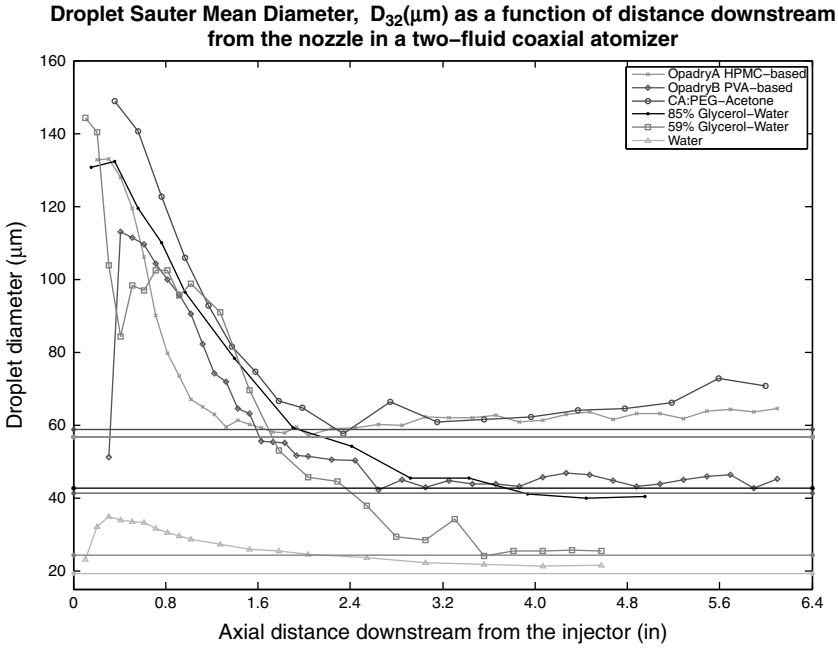

FIGURE 40.13 Droplet diameter versus axial distance downstream from the spray gun.

and are therefore more prone to radial excursions induced by small velocity fluctuations in that direction. Finally, there is typically an increase in the droplet size near the outer boundary of the jet. In swirled sprays, this is very acute and is caused by the centrifugal migration of large inertia droplets that sustain the initial azimuthal momentum longer and therefore travel farther distance radially. But even in non-swirled flows, the instability responsible for liquid breakup requires a radial velocity on the liquid that induces acceleration when it is exposed to the high-speed gas stream. Due to the natural stochastic distribution of this radial velocity, some liquid masses have high initial radial velocity and cross the gas jet quickly. Because of this, these droplets have reduced time of exposure to the high-speed gas stream, which decays exponentially in the radial direction, and have reduced breakup frequencies as a result. The tails of the radial velocity distribution are then responsible of those large droplets and their location in the outskirts of the spray.

The droplet sizes resulting from coaxial atomization of a low-speed liquid jet and a coaxial high-speed gas jet have been typically described in terms of lognormal or gamma distributions. If a specific distribution is used to characterize the spray, two or sometimes only one moment can be used to quantify the droplet size over its entire range.

40.4.1 Velocity Measurements

The velocity of the two phases present in the spray can be measured by the same phase Doppler technique as was used to determine the droplet diameter distribution. The basis for velocity measurements is the same as that for laser Doppler velocimetry. Taking advantage of the size measurements, the velocity data can be segregated for tracer droplets that represent the velocity of the carrier gas and the velocity of the larger droplets that, because of their inertia, do not track the gas velocity.

For a typical axisymmetric coaxial injector, the gas velocity behaves as a classical round jet. After a short development length, during which the flat top profile injected at the nozzle evolves to adjust to the boundary conditions, the flow dynamics become self-similar and the velocity profile Gaussian. In a coaxial atomizer, the gas jet flows through a ring-shaped nozzle that leaves inside space for the liquid nozzle. Given the small cross section necessary for the liquid injection, the gas coming out of the nozzle expands into the centerline so that at the end of the development length, the gas in the spray behaves exactly as a round jet. Figure 40.14 shows velocity measurements in an axisymmetric coaxial injector. The gas velocity can be fitted very accurately by a Gaussian profile. The velocity of the droplets tends to follow a very similar profile, but the magnitude of the velocity is slightly higher. Considering the inertia of the droplets and that the gas velocity is decreasing as it flows downstream from injection due to entrainment of ambient air, this is to be expected. Of particular interest is the strong deviation associated with the droplets near the edge of the jet. Those droplets, typically larger than the average across all radial positions, traverse the jet from the centerline to the edge with a significant radial velocity and therefore reach the region of very low gas velocity before they lose their forward

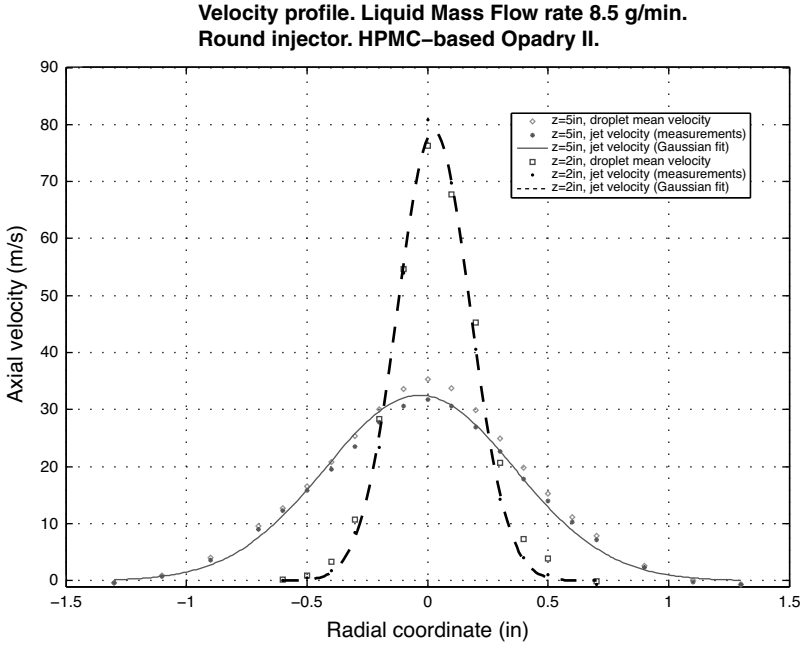

FIGURE 40.14 Droplet and gas jet velocity profile.

momentum. This produces the largest velocity difference between the two phases.

40.4.2 Effect of the Pattern Air on Turbulent Droplet Transport Within the Spray

The model for the breakup of the liquid jet into droplets does not take into account the existence of the two side jets that inject the pattern air into the spray.

The geometry of most pharmaceutical coating atomizers includes two auxiliary air jets that inject air from the edges of the liquid/air jet with a significant inward radial velocity component. Typical angles are between 30° and 45° with respect to the jet axial direction. Depending on the location and angle of the pattern air nozzles, these jets impinge on the droplet-laden jet after the liquid breakup process has finished or on the atomizing air as it is distorting the liquid jet. Pattern air plays an important role in the transport of the droplets of different sizes. Its effect on the liquid breakup is described in the next section. The goal of pattern air is to flatten the spray so that the spatial coverage of the atomizer in the coating pan is increased. To do this, the pattern air induces an asymmetry in the velocity field of the spray that makes its cross section become elliptical rather than circular. The spray is narrower along the axis of the side jets, where the pattern air momentum forces the spray inward (minor axis of the ellipse), and broader in the perpendicular axis (major axis of the ellipse). This is shown in Figure 40.15, where the size distribution is plotted in the radial direction along the minor and the major axis at two distances downstream of the injector. The effect of the pattern air on the droplet size distribution is rather complicated. First, the size distribution is concave along the major axis, and larger droplets are found as we move away from the axis due to the larger droplets conserving their radial momentum longer than the smaller ones. The contrary is true along the minor axis, where the effect of the side jets is more noticeable for the larger droplets that are subject to higher aerodynamic focusing toward the spray axis due to their larger inertia and lower diffusivity. The smallest droplets quickly adjust to the local gas velocity, minimizing any local perturbation inflicted by the pattern air. This explains the convex shape of the diameter distribution found along the cross-sectional minor axis. Furthermore, some very large droplets acquire a large radial velocity component as they interact with the side jets and, because of their large inertia, do not lose that momentum as they cross the spray axis. These droplets are then found in relatively high proportion in the outskirts of the jet, where the droplet number density is low and a small number of very large droplets have a significant impact on the average diameter of the distribution. This explains the change from convex to concave in the diameter radial distribution. Note that the inflexion point associated with this change in character moves outward from the spray axis with distance downstream, as one would expect those large droplets to keep moving in a radial direction, occupying the outer region of the spray. This inhomogeneity in the diameter distribution along the radial coordinate in the spray is a typical effect of pattern air that needs to be

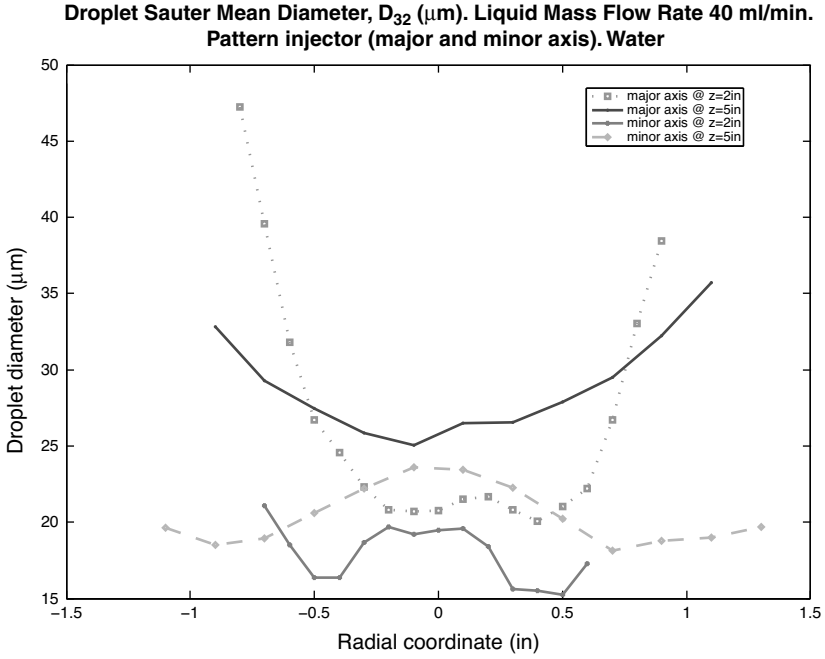

FIGURE 40.15 Droplet diameter versus radial distance from the center of the spray gun.

monitored to avoid large droplets accumulating at the edge of the spray.

40.5 MATHEMATICAL MODELING OF THE LIQUID BREAKUP: AVERAGE DROPLET SIZE

The atomization of a liquid jet by a coflowing, high-speed gas stream occurs via a series of fluid instabilities that lead to the disruption of the liquid jet and result in the liquid mass being broken into small spherical inclusions transported within a gas stream. Although the nature of the instability depends on the specific conditions present in the jet (Reynolds and Weber numbers, mass and dynamic pressure ratios between the air and liquid streams, etc.) and is the source of significant controversy, for the conditions typically present in pharmaceutical coating operations, it has been well documented ([9, 19]) that the breakup process follows a sequence of Kelvin–Helmholtz instability disrupting the liquid jet, followed by a Rayleigh–Taylor (RT) instability resulting in the breakup of the liquid cylinder into individual droplets. The Kelvin–Helmholtz instability develops in the annular shear layer that exists between the low-speed liquid injection and the high-speed coaxial gas jet. Once the liquid has been displaced from its axisymmetric position, it suffers a sudden acceleration as a result of the drag imposed by the gas flow and a Rayleigh–Taylor instability at the interface ensues. This process is shown in schematic form in Figure 40.16. The wavelength of the primary instability, λ_1, depends on the gas boundary layer thickness, δ_g, at the gas nozzle, as described by [20] and can be computed by the following equation:

$$\lambda_1 \approx 2\delta_g \sqrt{\frac{\rho_l}{\rho_g}} \tag{40.1}$$

where ρ_l and ρ_g are the liquid and gas densities, respectively. Spray atomization nozzles are typically designed with a strong convergence upstream of the nozzle so that the flow acceleration will keep the boundary layer laminar and, therefore, as thin as possible. The boundary layer thickness can then be calculated as

$$\delta_g = \frac{C b_g}{\sqrt{Re_{bg}}} \tag{40.2}$$

where $Re_{bg} \equiv U_{Gas} b_g / \nu_{Gas}$ and the coefficient of proportionality C depends on nozzle design. Considering air as the working gas and typical flow rates used in coating operations (1–5 SCFM, 20–100 SLPM), the Reynolds number is of order 10^4. The disrupted liquid mass is accelerated by the surrounding gas and its resulting convective velocity is

$$U_c = \frac{\sqrt{\rho_l} U_{Liquid} + \sqrt{\rho_g} U_{Gas}}{\sqrt{\rho_l} + \sqrt{\rho_g}} \tag{40.3}$$

For the Kelvin–Helmholtz instability to develop quickly, before the gas jet velocity decays and becomes close to the liquid injection velocity, the Reynolds number of the liquid shear layer must be large:

$$Re_{\lambda 1} = \frac{(U_c - U_{Liquid})\lambda_1}{\nu_l} > 10 \tag{40.4}$$

This condition is necessary even though the instability is driven by the gas. In the case of coating solutions that may have non-Newtonian rheology, the applicable viscosity, ν_l, is the effective shear viscosity at the injection shear rate.

The liquid excursions resulting from the K-H instability, of thickness b_l, grow rapidly and are exposed to and accelerated by the high-speed gas stream. This liquid is subsequently subject to a Rayleigh–Taylor instability similar to

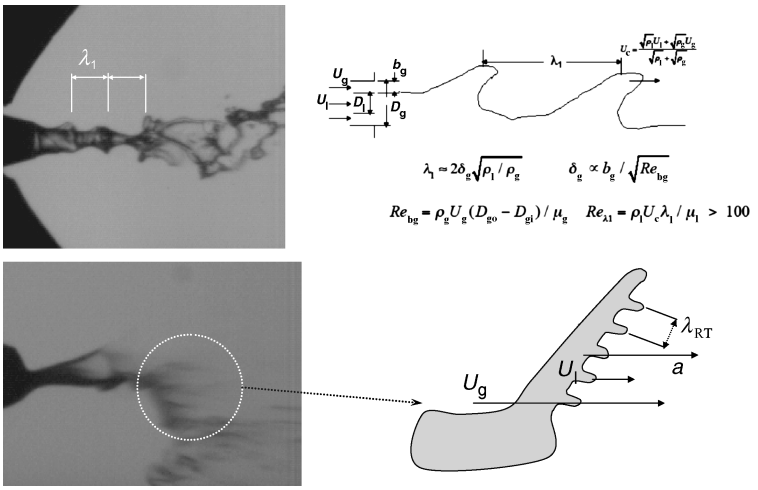

FIGURE 40.16 High-speed photograph (*top left*) and sketch (*top right*) of the primary Kelvin–Helmholtz instability. High-speed photograph (*bottom left*) and sketch (*bottom right*) of the secondary Rayleigh–Taylor instability.

water placed over oil. Because oil is lighter than water, the interface between the two liquids is accelerated and creates fingers by which oil flows up and water goes down. The growth of a R-T instability in an accelerated drop suddenly injected into a high-speed gas stream is studied in [21]. The dispersion relation for the case $\rho_g << \rho_l$ is given by

$$-\left[1+\frac{1}{n^2}\left(-ak+\frac{\sigma k^3}{\rho_l}\right)\right]+4\frac{k^2}{n}\frac{\alpha_l}{\rho_l} +4\frac{k^3}{n^2}\left(\frac{\alpha_l}{\rho_l}\right)^2(q_l-k)=0 \tag{40.5}$$

where k is the magnitude of the wave vector, n the amplification rate, a the acceleration of the liquid tongue, σ the surface tension, α_l the effective shear viscosity of the liquid in $\tau_{ij}=2\alpha_l e_{ij}$, where τ_{ij} and e_{ij} are, respectively, the stress and the rate of strain tensors in the liquid, and q_l is given by

$$q_l=\sqrt{k^2+n\rho_l/\alpha_l} \tag{40.6}$$

For very low Ohnesorge numbers, when viscous effects are negligible, the wave number corresponding to maximum amplification is

$$k_\sigma=\sqrt{\frac{a\rho_l}{3\sigma}} \tag{40.7}$$

This is the dominant case in water atomization and in fuel injectors where linear chain hydrocarbons with very low viscosity values are used, but it is rarely the case in coating operations where the coating solutions are typically high solid content solutions or particle dispersions with complex rheology.

When viscous terms are important, as is the case for the tablet coating operations, α_l is large and it can be assumed that $(n\rho_l/k^2\alpha_l) << 1$ such that $(q_l-k)\approx(n\rho_l/2k\alpha_l)$ in equation 40.6. The simplified dispersion relation from equation 40.5 then reads

$$n=-\frac{k^2\alpha_l}{\rho_l}\pm\sqrt{\frac{k^4{\alpha_l}^2}{\rho_l^2}-\left(\frac{k^3\sigma}{\rho_l}-ka\right)} \tag{40.8}$$

Disturbances will grow when the second term in equation 40.8 is positive and larger than the first term. It is useful to rewrite equation 40.8 in the following form:

$$n=\frac{k^2\alpha_l}{\rho_l}\left[\left(1+\frac{a\rho_l^2}{k^3\alpha_l^2}-\frac{\sigma\rho_l}{k\alpha_l^2}\right)^{1/2}-1\right] \tag{40.9}$$

From equation 40.9, the amplification rate is zero when $k=\sqrt{(a\rho_l/\sigma)}$, which is the capillary cutoff wave number, and when $k=0$. The wave number of maximum amplification is given by the third-order equation

$$4\frac{\alpha_l^2}{\rho_l^2}k^3-\frac{3\sigma}{\rho_l}k^2+a=0 \tag{40.10}$$

The exact solution of this equation is too complex to be of practical interest. However, for the high viscosity fluids typical of tablet coating, the Ohnesorge number (which controls the relative importance of liquid viscosity and surface tension, $Oh=\mu_l/\sqrt{\rho_l\sigma D_l}$) based on the wavelength is large and the second term in equation 40.10 is small compared to the first one, so that the wave number of maximum amplification is

$$k_{max}\approx\sqrt[3]{\frac{a\rho_l^2}{\alpha_l^2}} \tag{40.11}$$

The R-T wavelength is $\lambda_{RT}=2\pi/k_{max}$ and ultimately the droplet diameter is a fraction of λ_{RT} [19]. Therefore, assuming viscous and surface tension effects are additive to the leading order according to the dispersion relation, we look for a correlation in the following form:

$$\lambda_{RT}=2\pi\left[\sqrt{\frac{3\sigma}{a\rho_l}}+C_2\sqrt[3]{\frac{\alpha_l^2}{a\rho_l^2}}\right] \tag{40.12}$$

The acceleration a in equation 40.12 is simply $a=\frac{F}{m}=\frac{F}{\rho_l V}$, where the force F is the drag force exerted by the gas stream on a liquid element, and here the liquid tongue of the primary instability

$$F=\frac{1}{2}C_D\rho_g(U_{Gas}-U_c)^2A_e \tag{40.13}$$

where $C_D\approx 2$ is the drag coefficient and A_e the projected area. The mass of the liquid to be accelerated is $m=\rho_l b_l A_e$ with $b_l\propto\lambda_1$. The expression for a is therefore given by

$$a\approx\frac{\rho_g(U_{Gas}-U_c)^2}{\rho_l b_l} \tag{40.14}$$

Substitution of equation 40.14 in equation 40.12 gives

$$\lambda_{RT}\propto\left(\frac{\sigma\lambda_1}{\rho_g(U_g-U_c)^2}\right)^{1/2} \times\left(1+C_2'\left\{\frac{\rho_g(U_g-U_c)^2}{\lambda_1\sigma}\right\}^{1/6}\left\{\frac{\alpha_l^2}{\rho_l\sigma}\right\}^{1/3}\right) \tag{40.15}$$

Further substituting for λ_1 from equation 40.1, using equation 40.2, and taking the drop diameter, say the Sauter mean diameter (SMD), proportional to λ_{RT} gives

$$\frac{SMD}{D_l}=C_1(1+m_r)\left(\frac{b_g}{D_l}\right)^{1/2}\left(\frac{\rho_l/\rho_g}{Re_{bg}}\right)^{1/4}\frac{1}{\sqrt{We_{D_l}}} \times\left\{1+C_2\left(\frac{D_l}{b_g}\right)^{1/6}\left(\frac{Re_{bg}}{\rho_l/\rho_g}\right)^{1/12}We_{D_l}^{1/6}Oh^{2/3}\right\} \tag{40.16}$$

In equation 40.16, the mass loading effect in the form $(1 + m_r)$ is obtained from energy arguments previously outlined by [22], where $m_r = m_l/m_g = (\rho_l U_{Liquid} A_l)/(\rho_g U_{Gas} A_g)$ and A_l and A_g are the areas of the liquid and gas nozzle exit sections, respectively. Furthermore, this equation indicates a dependency of the SMD on $U_{Gas}^{-5/4}$ and $\sigma^{-1/2}$. The drop diameter increases with $b_g^{1/4}$ if the coefficient of proportionality C in equation 40.3 remains constant when b_g is changed. As will be shown below, this would be the case only if the length of the gas jet potential cone is much larger than the liquid jet's intact length, which is not typical of atomizer designs.

The SMD in equation 40.16 has been made dimensionless by the liquid orifice diameter D_l and the Weber and Ohnesorge numbers are based on D_l following the usual convention. However, it should be emphasized that the drop diameter does not depend on the liquid orifice diameter but rather on the gas boundary layer thickness at the nozzle exit. This has been clearly demonstrated by [19], where the liquid orifice diameter was changed by a factor of 3 and the drop diameter remained practically identical for the same gas flow conditions.

For completeness, the various nondimensional parameters in equation 40.16 are defined as follows:

$$\begin{aligned}
\text{Weber number}: \ We_{Dl} &= \frac{\rho_g (U_{Gas} - U_c)^2 D_l}{\sigma} \\
\text{Ohnesorge number}: \ Oh &= \frac{\alpha_l}{\sqrt{\rho_l \sigma D_l}} \\
\text{Reynolds number}: \ Re_{bg} &= \frac{U_{Gas} b_g}{\nu_g} \\
\text{Mass flux ratio}: \ m_r &= \frac{\rho_l U_{Liquid} A_l}{\rho_g U_{Gas} A_g}
\end{aligned} \tag{40.17}$$

The coefficients C_1 and C_2 in equation 40.16 are of order 1 and values for both coefficients are determined from experiments. The value of C_1 depends on the gas nozzle geometry in general, and on the contraction ratio in particular, because for a given nozzle size the gas boundary layer thickness at the liquid nozzle discharge depends strongly on the contraction ratio. C_2 characterizes the viscosity dependence of the critical wave number in the R-T instability, compared to the surface tension dependence. This value is associated to the additivity and linearity of both cohesive effects, surface tension, and viscosity, which determine the growth rate of the instability. The validity of the linear theory for R-T instability has been confirmed for a wide parameter range via qualitative observation of the jet breakup process.

Another important parameter that does not appear explicitly in equation 40.16 is the dynamic pressure ratio M that determines the rate of atomization and hence the intact length of the liquid stream [23].

This ratio is defined as

$$M = \frac{\rho_g U_{Gas}^2}{\rho_l U_{Liquid}^2} \tag{40.18}$$

The dimensionless intact length of the liquid stream can be defined as $L/D_l \approx 6/\sqrt{M}$ and in coaxial injectors used under usual tablet coating parameters, M is typically large (of the order of 100). The gas potential cone length is approximately $6b_g$. For efficient atomization, it is desirable that the gas potential cone length be equal to or larger than the liquid intact length so that the primary atomization is completed before the gas velocity starts to decrease. This requirement is expressed by

$$\frac{b_g \sqrt{M}}{D_l} > 1 \tag{40.19}$$

It is worth noting that for the flow rates and atomizers utilized in pharmaceutical tablet coating, equation 40.19 is satisfied easily, with values typically exceeding 10, strongly suggesting that atomization is typically quite rapid and efficient. Finally, the fluid jets under the conditions of interest here are laminar at the injector nozzle but would potentially become turbulent if the flow rates are significantly increased or the gas contraction ratio decreased. Turbulent conditions of the liquid stream at the nozzle discharge plane would have little effect on the atomization process, while turbulent conditions in the high-speed gas stream would require altering the exponent of Re_{bg} in equation 40.16.

40.5.1 Pattern Air Effect on the Liquid Breakup

The previous model is derived for two coaxial streams of liquid and air, without taking into account the effect of pattern air on the liquid breakup. The effect of pattern air can be included in the model in two different ways.

In spray guns where the pattern air nozzles are oriented in a way that the jets impinge on the spray axis at a distance from the atomization nozzle at which liquid breakup is already underway, the effect of pattern air on droplet size is minor. Because the droplet size is set by the wavelength of the secondary R-T instability, pattern air does not modify it when the instability is already growing. Therefore, for this type of atomizers, only the gas flow through the atomization nozzle affects the breakup. In atomizers where the pattern air comes from the same supply line as the atomizer air, the effect of pattern air is simply to reroute some of the available gases from the atomizing nozzle to the side jets, and therefore reducing the atomizing air flow rate and the exit velocity. To account for that, in the case when pattern air does not have independent flow control and measurements, it is easiest to measure the cross-sectional area of both the atomizing nozzle and the pattern air and to prorate the total flow rate into the two air streams according to the pressure loss across the two

nozzles (which is proportional to the diameter to the fourth power). The atomizing air is the value that is input into the breakup model, setting U_g and consequently the Weber number and the gas Reynolds number in the model.

In spray guns where the position and orientation of the pattern air nozzles result in the side jets impinging on the spray axis very close to the atomizing nozzle, in the region where the instability of the liquid jet is still developing, the impact of the pattern air jets on the droplet size resulting from the atomization is very strong. This effect can be modeled by considering that the atomizing air and the pattern air mix while the liquid jet is breaking up. The resulting air stream has axial momentum equal to the sum of all the jets but no radial momentum as the two pattern air side jets have equal but opposite values that cancel when the two streams mix. One can implement this into the previously derived model by computing the gas jet as the mean air velocity of the two streams, $U_g = (m_{atom}U_{atom} + m_{pattern}U_{pattern}\cos\theta)/(m_{atom} + m_{pattern})$, where θ is the angle between the pattern air jet axis and the atomizing air jet axis. Although there are a number of approximations underlying this model, most importantly that the air streams mix instantly and that the instability is not modified by the lack of axial symmetry induced by the pattern air, it has been proven to provide accurate predictions for the droplet size under typical pharmaceutical coating conditions.

40.6 SCALE-UP OF ATOMIZATION

The tablet coating process is often developed and optimized at a small scale and subsequently scaled up to larger equipment and batch size. The coating and atomization process are developed and optimized in a small lab coater, typically at 1–10 L capacity using a few kilograms of tablets, through detailed experimentation. The main goal of this experimentation is to explore the design space of the process parameters, such as the spray rate, atomization air flow rate, and pattern air flow rate, which will produce spray that will result in the desired film coat on the tablet surface. When this process is scaled up, process parameters should be selected such that coating spray will be similar to the one generated at the smaller scale.

An important spray characteristic that should be kept the same across different scale experiments is the SMD droplet size. In this example, equation 40.16 will be used to calculate the SMD for 1–2, 30, and 500 L coating pans based on the spray parameters given in Table 40.4. Furthermore, this

TABLE 40.4 Process Variables and Parameters for Spray Atomization for Three Different Scale Coaters Used in Scale-Up Example. Fluid Properties for Opadry II White (Colorcon Code: Y-30-18037)

Spray Parameters and Variables	1–2 L Scale	30 L Scale	500 L Scale
Input parameters			
Inner diameter of liquid nozzle (m)	1.00E − 03	1.50E − 03	1.50E − 03
Outer diameter of atomizing gas cap (m)	3.00E − 03	4.00E − 03	4.00E − 03
Inner diameter of atomizing gas cap (m)	2.00E − 03	3.00E − 03	3.00E − 03
Diameter of the pattern air side orifices (m)	1.0E − 03	2.0E − 03	2.0E − 03
Liquid surface tension (N/m)	0.047	0.047	0.047
Liquid density (kg/m^3)	1050.0	1050.0	1050.0
Infinite shear rate viscosity (kg/m s)	0.0981	0.0981	0.0981
Spray rate (g/min per spray gun)	10	60	120
Liquid mass flow rate (kg/s)	1.67E − 04	1.00E − 03	2.00E − 03
Air density (kg/m^3)	1.225	1.225	1.225
Air viscosity (kg/ms)	1.80E − 05	1.80E − 05	1.80E − 05
Gas volumetric flow rate (m^3/s)	1.18E − 03	2.92E − 03	3.41E − 03
Calculated values used in the model			
Liquid outlet velocity (m/s)	2.012E − 01	5.389E − 01	1.078E + 00
Gas outlet velocity (m/s)	214.61	247.97	289.63
Gas jet Reynolds number	7302.63	8437.946	9855.630
Convective velocity of the primary instability waves	7.284	8.711	10.608
Liquid Weber number	1120.311	2238.069	3043.828
Mass flux ratio	0.115	0.279	0.478
Dynamic pressure ratio	1315.525	246.988	84.239
Ohnesorge number	0.4416	0.3606	0.3606
Model output			
Sauter mean diameter (μm)	**48.4**	**48.4**	**48.4**

Note: Spray gun parameters are, for example purposes. They are not selected based on a specific spray gun model. Pattern air is not independent in this example.

TABLE 40.5 Impact of Coating Formulation Solids Content on the Mean Droplet Size (i.e., Sauter Mean Diameter) and Fluid Properties for Opadry II White (Colorcon Code: OY-LS-28914)

Spray Parameters and Variables	10% Solids	12% Solids	15% Solids
Input parameters			
Inner diameter of liquid nozzle (m)	1.20E – 03	1.20E – 03	1.20E – 03
Outer diameter of atomizing gas cap (m)	3.10E – 03	3.10E – 03	3.10E – 03
Inner diameter of atomizing gas cap (m)	2.60E – 03	2.60E – 03	2.60E – 03
Diameter of the pattern air side orifices (m)	1.50E – 03	1.50E – 03	1.50E – 03
Liquid surface tension (mN/m)	48.22	47.66	46.67
Liquid density (kg/m^3)	1020.0	1030.0	1040.0
Infinite shear rate viscosity (kg/m s)	0.095	0.181	0.419
Spray rate (g/min per spray gun)	60	60	60
Atomizing gas volumetric flow rate (m^3/s)	1.42E – 03	1.42E – 03	1.42E – 03
Calculated values used in the model			
Gas outlet velocity (m/s)	245.27	245.27	245.27
Model output			
Sauter mean diameter (μm)	**52.4**	**72.9**	**116.8**

Note: Spray gun parameters are, for example, purposes and are not selected based on a specific spray gun model. Pattern air is not independent in this example.

model will be used to set the atomization gas flow rate that will produce spray with same SMD for the given parameters.

In the example given in Table 40.5, the coating fluid solids content is increased from 10% to 12%, and then to 15%. This increase in % solids causes a dramatic change in fluid viscosity and also the droplet size as can be seen when equation 40.16 is used to predict droplet size. If atomization is left unchanged, the resulting droplet size of 116.8 μm from the 15% solids formulation would likely be too large. The model can then be used to determine the appropriate atomization air flow to achieve an acceptable droplet size.

TABLE 40.6 Impact of Coating Spray Gun Equipment Change on the Mean Droplet Size (i.e., Sauter Mean Diameter)

Spray Parameters And Variables	Spray Gun Setup 1 Process A	Spray Gun Setup 2 Process A	Spray Gun Setup 2 Process B
	Original Equipment and Process	Equipment Change/No Change in Process	Atomizing Gas Decreased to Match Droplet Size of Setup 1
Spray pattern type	Round	Ellipse	Ellipse
Fluid nozzle part #	PF2850	PF28100	PF28100
Air cap part #	120	PA110228-45	PA110228-45
Atomization air annulus (mm)	2.03	1.01	1.01
Input parameters			
Inner diameter of liquid nozzle (mm)	0.95	0.71	0.71
Outer diameter of the atomizing gas cap (mm)	3.33	2.79	2.79
Inner diameter of the atomizing gas cap (mm)	1.3	1.78	1.78
Diameter of the pattern air side orifices (m)	0	0.71	0.71
Liquid surface tension (mN/m)	43.9	43.9	43.9
Liquid density (kg/m^3)	1070.0	1070.0	1070.0
Infinite shear rate viscosity (kg/ms)	0.039	0.039	0.039
Spray rate (g/min per spray gun)	10	10	10
Atomizing gas volumetric flow rate (m^3/s)	1.18E – 03	1.18E – 03	6.65E – 04
Calculated values used in model			
Atomizing gas outlet velocity (m/s)	159.8	267.1	150.7
Model output			
Sauter mean diameter (μm)	**49.9**	**25.8**	**49.7**

Note: Fluid properties are for Opadry II White 20% solids (Colorcon Code: 85F18422). Example spray guns are available from Spraying Systems Co.

In the example given in Table 40.6, the coating process equipment is changed when product is processed with two coaters with different spray guns (i.e., setup 1 and setup 2). If the original process conditions (i.e., atomization gas volumetric flow rate) are kept and spray setup is changed from 1 to 2, the resulting droplet size is predicted to decrease from 49.9 to 25.8 μm due to differences in atomizer geometry. This reduction of droplet size may change coating appearance or influence efficiency of the coating process, and so the model can be used to predict the atomization air flow rate necessary to maintain the droplet size at about 50 μm (i.e., process B).

40.7 CONCLUSIONS

In this chapter, we have outlined the physical processes that are involved in the spray coating of pharmaceutical tablets. We have focused on the atomization of the complex rheology liquid formulations used in the coating because the size and spatial distribution of the droplets formed during the atomization process have a strong influence on the success or failure of the overall process. The essential physics of the problem have been described in detail and a mathematical model for the prediction of the average droplet size has been presented. The hydrodynamic stability analysis of the two parallel streams of gas and liquid characteristic of two-fluid atomizers, commonly used in the coating operations, provides quantification of the functional dependency of the resulting droplet size with the coating formulation properties (surface tension, viscosity) and the operational conditions (liquid and gas flow rates). We have also investigated the spatial distribution of droplets within the spray and the effect of the symmetry breaking side gas jets (commonly referred to in the industry as pattern air). We show the redistribution of droplets into an elliptical cross section spray due to these side jets and a more uniform spray density. The conditions under which these side jets need to be taken into account in the calculation of the droplet size have been identified and a simple way to include them in the breakup model is presented.

The availability of quantitative, physics-based models such as the one presented in this chapter can change the way pharmaceutical manufacturing operations, like tablet coating, is approached. The capability of predicting droplet size and distribution onto the coated material allows the optimization of the process with reduced input from experiments, as opposed to the traditional empirical approach that requires costly and time-consuming tests at each step of the process design (lab, pilot, and full scale). The improved understanding of the relationship between coating liquid rheology and coating outcomes can also provide more flexibility in the use of advanced coating formulations, reducing the barriers to apply novel coatings to improve a product or process.

ACKNOWLEDGMENTS

The authors would like to acknowledge Pfizer Inc. for supporting the research reported in this chapter. In addition, Douglas M. Kremer is thanked for his contributions to set up and develop this collaborative research effort. We also wish to thank Dr. Emil Hopfinger for his assistance in developing the atomization model described in Section 40.6. Katie Osterday is acknowledged for assisting in the viscosity measurements as well as in the measurements of the droplet size distributions using PDPA techniques. Daniel Bolleddula is acknowledged for helping set up the two-fluid coaxial atomizers for the independent pattern air experiments.

REFERENCES

1. Smith GW, Macleod GS, Fell JT. Mixing efficiency in side-vented coating equipment. *AAPS PharmSciTech*, 2003;4(3): E37.
2. am Ende MT, Berchielli A. A thermodynamic model for organic and aqueous tablet film coating. *Pharm. Dev. Technol.*, 2005;10(1):47–58.
3. Kalbag A, et al. Inter-tablet coating variability: residence times in a horizontal pan coater. *Chem. Eng. Sci.*, 2008;63(11): 2881–2894.
4. Ebey GC. A thermodynamic model for aqueous film-coating. *Pharm. Technol.*, 1987;11(4):40, 42–43, 46, 48, 50.
5. Porter SC, Felton LA. Techniques to assess film coatings and evaluate film-coated products. *Drug Dev. Ind. Pharm.* 36(2): 128–142.
6. McGinity JW, Felton LA, editors, *Aqueous Polymeric Coatings for Pharmaceutical Dosage Forms*, 3rd edition, Informa Healthcare, 2008, p. 488.
7. Turton R, Cheng XX. The scale-up of spray coating processes for granular solids and tablets. *Powder Technol.*, 2005;150(2): 78–85.
8. Gibson SHM, Rowe RC, White EFT. Mechanical properties of pigmented tablet coating formulations and their resistance to cracking. I. Static mechanical measurement. *Int. J. Pharm.*, 1988;48(1–3):63–77.
9. Aliseda A, et al. Atomization of viscous and non-Newtonian liquids by a coaxial, high-speed gas jet. Experiments and droplet size modeling. *Int. J. Multiphase Flow*, 2008;34 (2):161–175.
10. Mueller R, Kleinebudde P. Comparison of a laboratory and a production coating spray gun with respect to scale-up. *AAPS PharmSciTech*, 2007;8(1):3.
11. Mueller R, Kleinebudde P. Comparison study of laboratory and production spray guns in film coating: effect of pattern air and nozzle diameter. *Pharm. Dev. Technol.*, 2006. 11(4):425–433.
12. Tobiska S, Kleinebudde P. Coating uniformity: influence of atomizing air pressure. *Pharm. Dev. Technol.*, 2003;8(1): 39–46.

13. Thombre AG, et al. Osmotic drug delivery using swellable-core technology. *J. Control. Release*, 2004;94(1):75–89.
14. Thombre AG, et al. Asymmetric membrane capsules for osmotic drug delivery. II. In vitro and in vivo drug release performance. *J. Control. Release*, 1999;57(1):65–73.
15. Cole G, Hogan J, Aulton ME. *Pharmaceutical Coating Technology*, Informa Healthcare, 1995.
16. de Gennes PG, Brochard-Wyart F, Quéré D. *Capillary and Wetting Phenomena: Drops, Bubbles, Pearls, Waves*, Springer, 2002.
17. Bachalo WD. Experimental methods in multiphase flows. *Int. J. Multiphase Flow*, 1994;20 (Suppl.):233–259.
18. Williams FA. *Combustion Theory*, 2nd edition, Addison Wesley, 1985.
19. Varga CM, Lasheras JC, Hopfinger EJ. Initial breakup of a small-diameter liquid jet by a high speed gas stream. *J. Fluid Mech.*, 2003;497:405–434.
20. Marmottant P. *Atomisation d'un courant liquide dans un courant gazeux*, Institut National Polytechnique de Grenoble, Grenoble, 2001.
21. Joseph DD, Beaver GS, Funada T. Rayleigh–Taylor instability of viscoelastic drops at high Weber numbers. *J. Fluid Mech.*, 2002;453:109–132.
22. Mansour A, Chigier N. Air-blast atomization of non-Newtonian liquids. *J. Non-Newtonian Fluid Mech.*, 1995;58:161–194.
23. Lasheras JC, Hopfinger EJ. Liquid jet instability and atomization in a coaxial gas stream. *Ann. Rev. Fluid Mech.*, 2000;32: 275–308.